Structure, Volume *23*

Supplemental Information

Structural Insights into Ca^{2+}-Calmodulin Regulation of Plectin 1a-Integrin β4 Interaction in Hemidesmosomes

Jae-Geun Song, Julius Kostan, Friedel Drepper, Bettina Knapp, Euripedes de Almeida Ribeiro, Jr., Petr V. Konarev, Irina Grishkovskaya, Gerhard Wiche, Martin Gregor, Dmitri I. Svergun, Bettina Warscheid, and Kristina Djinović-Carugo

Supplementary information

Structural insights into Ca^{2+}/calmodulin regulation of plectin 1a - integrin β4 interaction in hemidesmosomes

Jae-Geun Song[1], Julius Kostan[1], Friedel Drepper[2], Bettina Knapp[2], Euripedes de Almeida Ribeiro Jr[1], Petr V. Konarev[3], Irina Grishkovskaya[1], Gerhard Wiche[4], Martin Gregor[5], Dmitri I. Svergun[3], Bettina Warscheid[2] and Kristina Djinović-Carugo[1,6]

[1]Department of Structural and Computational Biology, Max F. Perutz Laboratories, University of Vienna, Campus Vienna Biocenter 5, A-1030 Vienna, Austria

[2]Department of Functional Proteomics and Biochemistry, Institute of Biology II and BIOSS Centre for Biological Signaling Studies, University of Freiburg, Schaenzlestrasse 1, D-79104 Freiburg, Germany

[3]EMBL-Hamburg c/o DESY, Notkestrasse 85, D-22603, Hamburg, Germany

[4]Department of Biochemistry and Cell Biology, Max F. Perutz Laboratories, University of Vienna, A-1030 Vienna, Dr. Bohrgasse 9, Austria

[5]Department of Integrative Biology, Institute of Molecular Genetics of the ASCR, Vídeňská 1083, Prague 4, CZ-14220, Czech Republic

[6]Department of Biochemistry, Faculty of Chemistry and Chemical Technology, University of Ljubljana, Aškerčeva 5, SI-1000 Ljubljana, Slovenia

*Corresponding author: Kristina Djinović-Carugo (e-mail: kristina.djinovic@univie.ac.at)

Supplementary Information

Materials and Methods

Protein Cloning, Expression and Purification

The murine plectin construct (P1aABD, 1-263) contains the N-ter tail and the actin-binding domain (ABD) of plectin isoform 1a (Uniprot accession number: **Q9QXS1-3**). The truncation mutants of P1aABD were generated to express various lengths of the N-ter segment, and were named P1aABD$_{\Delta 11}$ (12-263), P1aABD$_{\Delta 22}$ (23-263), P1aABD$_{\Delta 32}$ (33-263), and P1aABD$_{\Delta 37}$ (38-263). The integrin β4 construct termed β4Fn12 (1126-1355) comprises the first pair of fibronectin type III domains including a part of the connecting segment (CS) of integrin β4 (Niessen et al., 1997) and was cloned using the cDNA of human integrin β4 (Rezniczek et al., 1998). The full-length calmodulin construct (CaM, 1-148) and its truncated versions encoding the N-ter and C-terminal lobes (CaM$_{NL}$ (6-73) and CaM$_{CL}$ (83-148), respectively) were prepared by cloning the entire human CaM gene III (Uniprot accession number: **P62158**). To generate constructs for heterologous expression in *E. coli*, plectin, calmodulin, and integrin β4 cDNAs were cloned into the pETM-14 vector, which encodes an N-ter His$_6$-tag and the 3C protease cleavage site.

An expression plasmid CaM-YFP (pMG13) encoding C-terminally EYFP-tagged calmodulin was generated by subcloning cDNA for human CaM gene III (a gift from D.C. Chang, Hong Kong University, China) into pEGFP-N2 -based plasmid (Clontech Laboratories, Inc.), where enhanced GFP had been replaced by EYFP (pEYFP). For cloning P1aABD-CFP (pMG39) encoding C-terminally ECFP-tagged plectin 1aABD, cDNA encoding a plectin fragment corresponding to exons 1a-8 (1aABD) (Kostan et al., 2009) was subcloned into pECFP-N2 plasmid which was generated using the same cloning strategy as pEYFP (see above). The YFP- and CFP-encoding plasmids were kindly provided by R. Tsien (University of California, San Diego, USA). The expression plasmid encoding CFP-YFP fusion was gift from D. Stanek (Institute of Molecular Genetics, Academy of Sciences of the Czech Republic, Czech Republic).

Oligonucleotide primers were designed to mutate two hydrophobic residues (Leu25Asp and Val29Asp) in the N-ter tail of plectin 1a. The PCR was carried out using the pMG39 vector mentioned above and the mutagenesis oligonucleotide primers (LVDD-F: 5‘ AGCTCAGAGGACAACGACTACCTGGCTGACCTCAGA GCCTCCGAG and LVDD-R: 5’ CTCGGAGGCTCTGAGGTCAGCCAGGTAGTCGTTGTCCTCTGAGCT). The amplified vector was incubated with *Dpn*I at 37 °C for 1 h to digest the template plasmid, followed by the transformation of competent *E.coli* DH5α cells.

The proteins were overexpressed in *E. coli* Rosetta2 (DE3) pLysS cells at 18 °C for 16 h after IPTG induction once the population reached an OD 600 of 0.6. Cells were lysed by sonication and protein purification was carried out using a 5 ml HisTrap HP column (GE Healthcare). To remove the His_6-tag, proteins were dialyzed against buffer containing 20 mM Tris-HCl pH 7.5, 500 mM NaCl, 0.1 mM EDTA, and 2 mM β-mercaptoethanol, and incubated with GST-3C protease. After a second nickel-affinity chromatography step, used to remove uncleaved protein, cleaved protein was further purified by gel filtration using a Superdex 75 16/600 column (GE Healthcare) equilibrated with 20 mM Tris-HCl pH 7.5, 150 mM NaCl, and 0.1 mM EDTA. To remove GST-3C protease from the sample, 5ml GSTrap HP column (GE Healthcare) was connected in series with the gel filtration column.

Small Angle X-ray Scattering (SAXS)

SAXS experiments on the P1aABD/CaM complex were performed using the SAXS beamline X33 at DESY (Hamburg, Germany) (Blanchet et al., 2012). The protein complex was purified by size-exclusion chromatography using a Superdex 75 16/60 column (GE Healthcare) after mixing P1aABD and CaM in an equal molar ratio. Protein samples were prepared in three different concentrations (3.5, 6.0, and 8.4 mg/ml) in the SAXS buffer (20 mM Tris-HCl pH 7.5, 150 mM NaCl, 5 mM $CaCl_2$, and 1 mM DTT). Structural parameters, zero-angle intensity (I(0)) and radius of gyration (Rg), from the Guinier plot were calculated using PRIMUS (Konarev et al., 2003). The program GNOM was employed to generate the pair distribution curve for determining the maximum dimension (D_{max}) and to obtain Rg and I(0) values (Svergun, 1992). *Ab initio* shape determination was computed by the program DAMMIF (Franke and Svergun, 2009) and generated dummy models were averaged using the program DAMAVER (Volkov and Svergun, 2003). Rigid-body modeling of the complex was performed by the program CORAL (Petoukhov et al., 2012) employing two subunits - one is the crystal structure of the $P1aABD_{\Delta 22}/CaM_{NL}$ complex and the other is the crystal structure of CaM_{CL} (83-148, PDB: 3CLN) (Babu et al., 1988), which was combined with an *ab initio* approach to model missing residues (1-21 residues of P1aABD and 74-82 residues of CaM).

SAXS data of the P1aABD/β4Fn12 complex were collected at SWING beamline in the synchrotron SOLEIL (Saint-Aubin, France) (David and Perez, 2009) and processed using the program Foxtrot. The protein complex was prepared by mixing P1aABD and β4Fn12 in an equal molar ratio with three concentration

series (2.4, 4.5, and 6.9 mg/ml) containing the SAXS buffer lacking $CaCl_2$. *Ab initio* structure determination of the P1aABD/β4Fn12 complex was performed in the same way as for the P1aABD/CaM complex. The program OLIGOMER (Konarev et al., 2003) was employed to calculate the volume fraction of the P1aABD/β4Fn12 complex in solution to account for its partial dissociation for the concentrations used. The residues missing in the crystal structure of the $P1aABD_{\Delta 22}$/β4Fn12 complex (1-37 residues of P1aABD and 1321-1355 residues of β4Fn12) were modeled by the program BUNCH (Petoukhov et al., 2012) before generating form factors for OLIGOMER analyses.

EOM (Ensemble optimization method) was employed to assess the flexibility of the N-ter tail of P1a (Bernado et al., 2007). Three concentrations of P1aABD samples (3.0, 4.5, and 6.0 mg/ml) were measured at the SAXS beamline X33 at the DORIS III storage ring, DESY (Hamburg, Germany) (Blanchet et al., 2012). The random pool of 10,000 conformers was generated to model the N-ter tail using the crystal structure of plectin ABD as a constraint. 50 models in the pool were selected to calculate the averaged scattering intensity (termed as selected ensemble), which was fitted to experimental data. Rg distributions against the frequency of occurrence were analyzed and compared between the pool and the selected ensemble.

Cross-Linking and Mass Spectrometry Analyses

Cross-linking experiments were performed using both a one-step and a two-step protocol. For the one-step method, 2 mM 1-ethyl-3-(3-dimethylaminopropyl)carbodiimide (EDC) and 5 mM N-hydroxysulfo-succinimide (sulfo-NHS) were added to the mixture of P1aABD and CaM (5 µM each prepared in the reaction buffer I consisting of 0.1 M MES-NaOH pH 6.5, 0.5 M NaCl and 2 mM $CaCl_2$) or to the mixture of P1aABD and β4Fn12 (5 µM each prepared in the reaction buffer II consisting of 20 mM HEPES pH 7.5, 50 mM NaCl) and incubated for 30 min at RT. For the two-step cross-linking method, 5 µM CaM or 5 µM β4Fn12 were prepared in the reaction buffer I and II, respectively, and activated with 2 mM EDC and 5 mM sulfo-NHS for 15 min at RT followed by the addition of 20 mM β-mercaptoethanol to quench excessive EDC. Subsequently, P1aABD prepared in the respective reaction buffer was added to the activated protein (CaM or β4Fn12) in equal molar ratio and incubated for 30 min at RT.

Following separation of cross-linking samples by SDS-PAGE and staining of proteins with colloidal Coomassie Blue G-250, protein bands were excised, subjected to in-gel digestion using trypsin and

analyzed by nano-HPLC-ESI-MS/MS using an UltiMate 3000 RSLCnano/LTQ-Orbitrap XL system (Thermo Fisher Scientific, Bremen, Germany) as described (Cristodero et al., 2013). In a first step, data files from LC-MS/MS measurements were analyzed by standard database searches using the programs OMSSA (version 2.1.9) (Geer et al., 2004) and MaxQuant (version 1.3.0.5) (Cox et al., 2011). All searches were done against the amino acid sequences for the recombinant proteins and for a set of common contaminants as provided with the distribution of the MaxQuant program with tryptic specificity allowing up to two missed cleavages. Oxidation of methionine and carbamidomethylation of cysteine residues were considered as variable and fixed modification, respectively. The mass tolerance for precursor ions was set to 5 ppm and for fragment ions to 0.5 Da. Match between runs was applied with a tolerance in retention time of 2 min. In a second step, data were subjected to a stringent search for the identification of cross-linked peptides using in-house developed programs. For this purpose, theoretical tryptic peptides of the recombinant proteins were computed with accurate masses and stored as an indexed table in a MySQL database. For each theoretical peptide, the difference between its accurate mass and the precursor mass of each MS/MS spectrum was computed and queried against the list of peptides indexed by mass using the same mass tolerances as in the first search. The cross-linker specificity was taken into account by retrieving only peptide pairs containing at least one suitable residue on each peptide.

For those peptide pairs matching an accurate precursor mass, the list of theoretical fragment ions was generated and compared to the experimental list of fragment ions. P-values were assigned using the formula used for the Andromeda score (Cox et al., 2011) with minor changes as specified in the following. Neutral losses were considered for the precursor mass but not for fragment masses. Charges of fragment ions were allowed from +1 up to the charge of the precursor minus 1, but only if the charge state was within a tolerance of +/- 1 of the expected charge state based on the number of charged groups in the respective fragment. The expected charge state of fragment ions was computed as the number of basic sites estimated according to a simple scheme (Arg, Lys, N-term: 1; His: 0.5) (Schlosser et al., 2007). $P_{\alpha/\beta}$-values were determined analogously to the calculation of the overall P-value of a cross-linked peptide spectrum match. These values represent the probability of finding at least the number of matched out of the number of theoretical fragment masses by chance for the α-/β-peptide of the cross-linked pair carrying the mass of the complementary peptide at one linkage residue. From the resulting

list of candidate peptide pairs, only those with $P_{\alpha/\beta}$-values below 0.05 were considered as cross-linked peptide spectrum matches.

Quantitative analysis of peptide spectrum matches was performed based on the intensities of peptide features in the allPeptides.txt result file from the MaxQuant program. For this purpose, the text file was stored in a MySQL table. For each peptide spectrum match, the sum of intensities was retrieved for features within the given precursor *m/z*-tolerance and +/- 1 min around the retention time at which the MS/MS spectrum was recorded.

Förster Resonance Energy Transfer (FRET) Experiments

Rat bladder carcinoma 804G cells were grown in Dulbecco's Modified Eagle's Medium (DMEM; Sigma Aldrich) medium, supplemented with 10% heat-inactivated fetal bovine serum and 1% penicillin/streptomycin (both PAA Laboratories). Cells were cultured at 37°C in 5% CO_2 and passaged every third day. Transient transfections of 804G cells were carried out in serum-free media using X-tremeGENE HP (Roche) according to the manufacturer's instructions with 2 µg plasmid and a 1:3 (w/v) ratio of DNA to transfection reagent. Cells were incubated with the transfection complexes for 24 hours and fixed in 4% paraformaldehyde/PIPES (Sigma Aldrich) for additional 24 h. After rinsing with Mg-PBS (phosphate-buffered saline supplemented with 10 mM Mg^{2+}) and water, cells were embedded in glycerol containing 1,4-diazabicyclo[2.2.2]octane (DABCO). FRET was measured by the acceptor photobleaching method as previously described (Stanek and Neugebauer, 2004) using the Leica SP5 confocal microscope. Intensities of CFP (excited by 405 nm laser set to 5–10% of maximum power) and YFP (excited by 514 nm laser line set to 2% of maximum power) were measured. Following this, YFP was bleached in a region of interest by three to five intensive (30% maximum power) pulses of 514 nm laser line and CFP and YFP fluorescence measured again. Apparent FRET efficiency was calculated according to the equation:

$$FRET_{efficiency}\ (\%) = (CFP_{after} - CFP_{before}) \times 100/CFP_{after}$$

Unbleached regions of the same cell were used as a negative control. Only cells displaying similar YFP and CFP signals were measured and cells not matching this criterion were omitted from the analysis. FRET efficiency is given throughout the text as mean ± SEM.

Supplementary Tables

Supplementary Table 1. (Supporting Figure 2)

Zero-length cross-link sites identified for complexes of P1aABD with CaM or integrin β4

Mass / Da	Peptide of P1aABD			Cross-linked peptide						Sum of Intensity
	Sequence [a]	Site	P-value [b]	Construct	Sequence [a]	Site	P-value [b]	P-value [c]	No. of spectra [d]	
1955.9565	ASEGKKDER	K36	6.7E-03	CaM	EAFSLFDK	E15	8.4E-14	4.7E-15	2	8.4 E6
2372.1453	KDER	K37	1.3E-03	CaM	EAFSLFDKDGDGTITTK	E15	7.9E-11	8.4E-14	1	2.1E6
2643.2760	KDERDR	K37	1.6E-03	CaM	EAFSLFDKDGDGTITTK	E15	7.4E-08	5.2E-12	3	8.4E6
1555.7858	ASEGKK	K36	1.9E-03	CaM	EAFSLFDK	E15	1.9E-07	2.0E-11	1	3.0E6
2844.3763	ASEGKKDER	K36	2.8E-02	CaM	EAFSLFDKDGDGTITTK	E15	7.7E-16	1.5E-17	2	7.8E7
1818.8752	EKGR	K92	2.1E-02	CaM	LTDEEVDEMIR	E121	3.2E-12	7.2E-14	1	2.3E6
1818.8766	EKGR	K92	1.5E-02	CaM	LTDEEVDEMIR	E124	1.0E-09	1.3E-11	1	1.8E6
2211.1308	HLIKAQR	K58	1.1E-04	CaM	LTDEEVDEM*IR	E124	2.8E-05	2.9E-10	2	6.6E6
1320.6529	KDERDR	K37	1.0E-03	CaM	EAFR	E88	3.7E-02	2.5E-06	1	1.5E5
1049.5253	KDER	K37	2.5E-02	CaM	EAFR	E88	3.0E-03	2.4E-05	1	8.3E4
1521.7516	ASEGKKDER	K36	1.3E-04	CaM	EAFR	E88	1.9E-02	5.8E-06	2	1.9E6
1513.7656	EKGR	K92	2.1E-02	CaM	HVM*TNLGEK	E115	3.5E-03	6.0E-05	2	1.1E6
1815.9627	KDERDR	K37	1.9E-03	β4Fn12	M*LLIENLR	E161	3.0E-09	2.5E-12	2	9.1E6
1544.8339	KDER	K37	5.9E-04	β4Fn12	M*LLIENLR	E161	4.0E-08	3.6E-11	4	9.3E6
1616.8907	ASEGKK	K36	2.2E-04	β4Fn12	M*LLIENLR	E161	5.4E-07	1.3E-11	2	1.0E7
2001.0679	ASEGKKDER	K36	1.3E-04	β4Fn12	MLLIENLR	E161	5.4E-07	5.0E-11	4	4.1E7

[a] E, K signify site of cross-linker, M*, oxidized methionine
[b] Subscores per peptide
[c] P-value for cross-linked peptide
[d] MS/MS spectra for ion species differing in charge or oxidation state; mass and P-values represent best match

174 ***Supplementary Table 2. (Supporting Figures 3-5)***

175 **SAXS Data-collection and structural parameters**

Sample	**P1aABD/CaM complex**	**P1aABD/β4Fn12 complex**	**P1aABD**
Data collection parameters			
Instrument	SAXS beamline X33 (DESY)	SWING beamline at the synchrotron SOLEIL	SAXS beamline X33 (DESY)
Sample to detector distance (m)	2.7 m	1.8 m	2.7 m
Wavelength (Å)	1.5	1.03	1.5
S range ($Å^{-1}$)	0.08-0.6	0.04-0.38	0.08-0.6
Exposure time (sec)	15	500	15
Temperature (K)	283	283	283
Structural parameters			
$I(0)$ [from $P(r)$]	47.44 ± 0.01	0.0429 ± 0.0001	26.05 ± 0.01
R_g (nm) [from $P(r)$]	3.17± 0.01	2.90 ± 0.01	2.51 ± 0.01
$I(0)$ (from Guinier)	47.94 ± 0.11	0.0430 ± 0.0057	26.29 ± 0.04
R_g (nm) (from Guinier)	3.17 ± 0.01	2.85 ± 0.6	2.52 ± 0.01
D_{max} (nm)	10.5	9.0	8.8
Porod volume estimate (nm^3)	79.33	55.01	60.91

176 Data are expressed as mean values ± standard deviation.

177

178 ***Supplementary Table 3. (Supporting Results section "Calmodulin Binds to Plectin 1a in an***
179 ***Extended Conformation)***
180
181 **Results of the PBD search for complexes where Ca^{2+}-CaM binds to the interaction partner in**
182 **an extended conformation.**
183
184

PDB	Year of deposition	Name	CaM conformation	Binding *via*
4R8G	2014	Crystal Structure of Myosin-1c tail in complex with Calmodulin	Extended	C-lobe
4BYF	2014	Crystal structure of human Myosin 1c in complex with calmodulin in the pre-power stroke state	Extended	C-lobe
2MGU	2014	Structure of the complex between calmodulin and the binding domain of HIV-1 matrix protein	Extended	Both lobes
4L79	2014	Crystal Structure of nucleotide-free Myosin 1b residues 1-728 with bound Calmodulin	Extended	C-lobe
4DCK	2012	Crystal structure of the C-terminus of voltage-gated sodium channel in complex with FGF13 and CaM	Extended	C-lobe
3SJQ	2012	Crystal structure of a small conductance potassium channel splice variant complexed with calcium-calmodulin	Extended	Both lobes

185
186
187

188 ***Supplementary Table 4. (Supporting Results section "Molecular Determinants of Integrin β4***

189 ***Displacement from the Complex with Plectin 1a by Calmodulin)***

190 **PISA binding interface analyses (Krissinel and Henrick, 2007)**

	$P1aABD_{\Delta22}/CaM_{NL}$		**$P1aABD_{\Delta22}/CaM_{CL}$**		**$P1aABD_{\Delta22}$/β4Fn12**	
	$P1aABD_{\Delta22}$	**CaM_{NL}**	**$P1aABD_{\Delta22}$**	**CaM_{CL}**	**$P1aABD_{\Delta22}$**	**β4Fn12**
Number of atoms	56 (2.8 %)	61 (12.3 %)	57 (2.9 %)	70 (13.3 %)	82 (4.4 %)	75 (5.0 %)
Number of residues	15 (6.2 %)	19 (29.2 %)	15 (6.2%)	23 (35.4 %)	21 (9.3 %)	24 (12.4 %)
Solvent-accessible area ($Å^2$)	665 (5.2 %)	635 (14.9 %)	671 (5.3%)	617 (13.4 %)	700 (5.9 %)	700 (6.3 %)
Solvation energy gain (kcal/mol)	-6.2 (2.9 %)	-6.7 (14.7 %)	-5.2 (2.4 %)	-5.4 (11.2 %)	0.7 (-0.4 %)	-0.1 (0.1 %)
P-value	0.006	0.140	0.021	0.075	0.527	0.591

191

192

Supplementary Figures

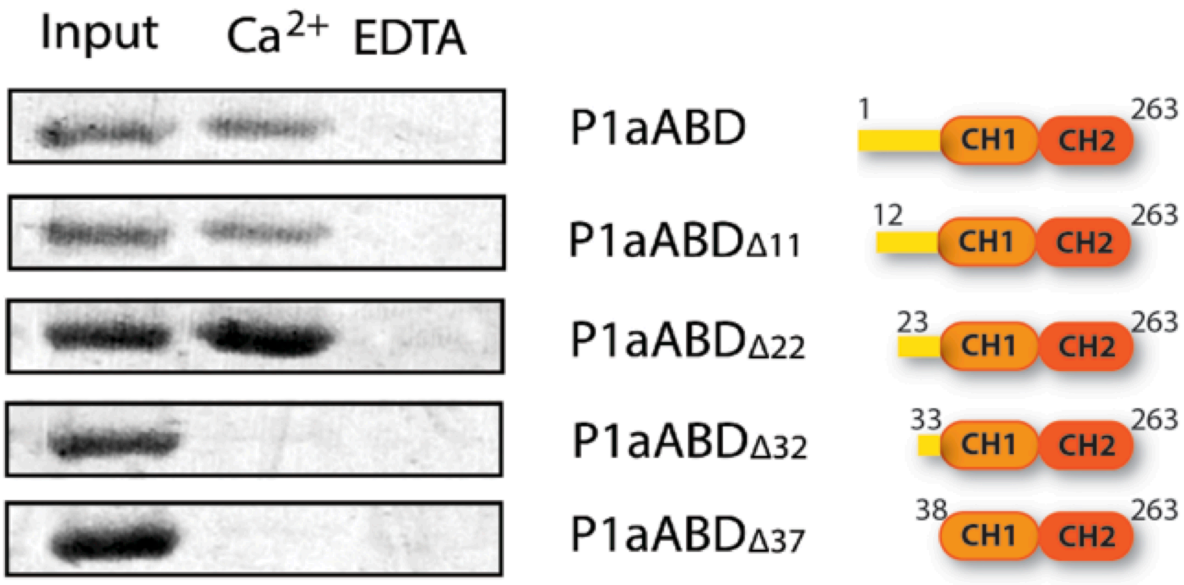

Supplementary Figure 1. (Supporting Results section "Plectin 1a Interacts with the N-ter Lobe of Calmodulin")

Pull-down assay was carried out using CaM-Sepharose beads in the presence of either calcium or EDTA. P1aABD$_{\Delta 22}$, the shortest plectin fragment displaying Ca^{2+}-dependent binding to CaM-Sepharose, was selected for the crystallization trials. Schematic representations show fragments used in the assay.

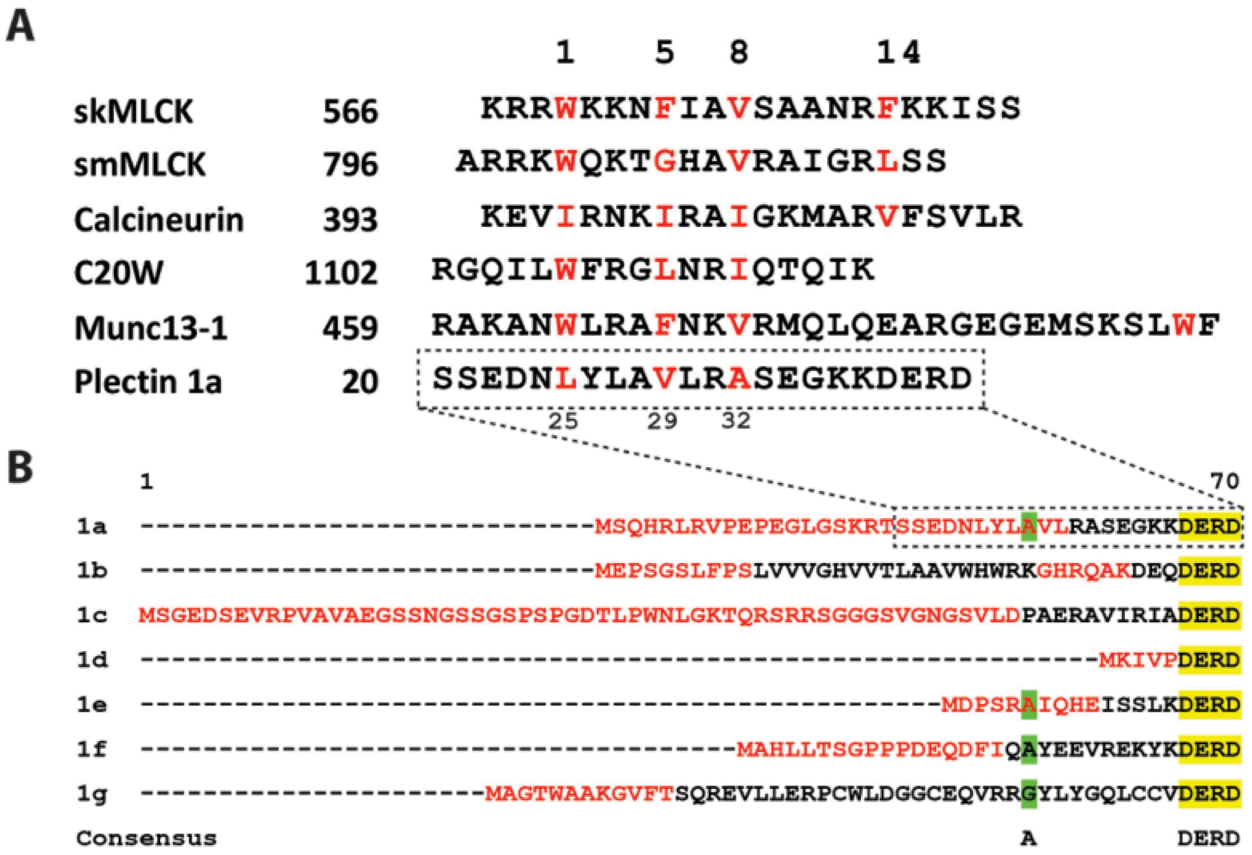

Supplementary Figure 2. (Supporting Results sections "Crystal Structure of the Plectin 1a ABD in Complex with Calmodulin N-ter Lobe" and "Calmodulin Binds to Plectin 1a in an Extended Conformation")

(A) Sequence alignment of CaM binding motifs. The hydrophobic residues corresponding to the CaM binding motifs are highlighted in red. skMLCK, smMLCK, and calcineurin are classified into a 1-5-8-14 motif, whereas C20W and plectin 1a belong to a 1-5-8 motif. Munc13-1 has a 1-5-8-26 CaM-binding motif. (B) The sequence alignment of plectin isoforms. The N-terminal specific sequences of seven isoforms were aligned, showing no sequence similarity among isoforms; conserved residues are shaded in green and identical residues are lightened in yellow. In addition, disordered residues predicted by PrDOS are shown in red.

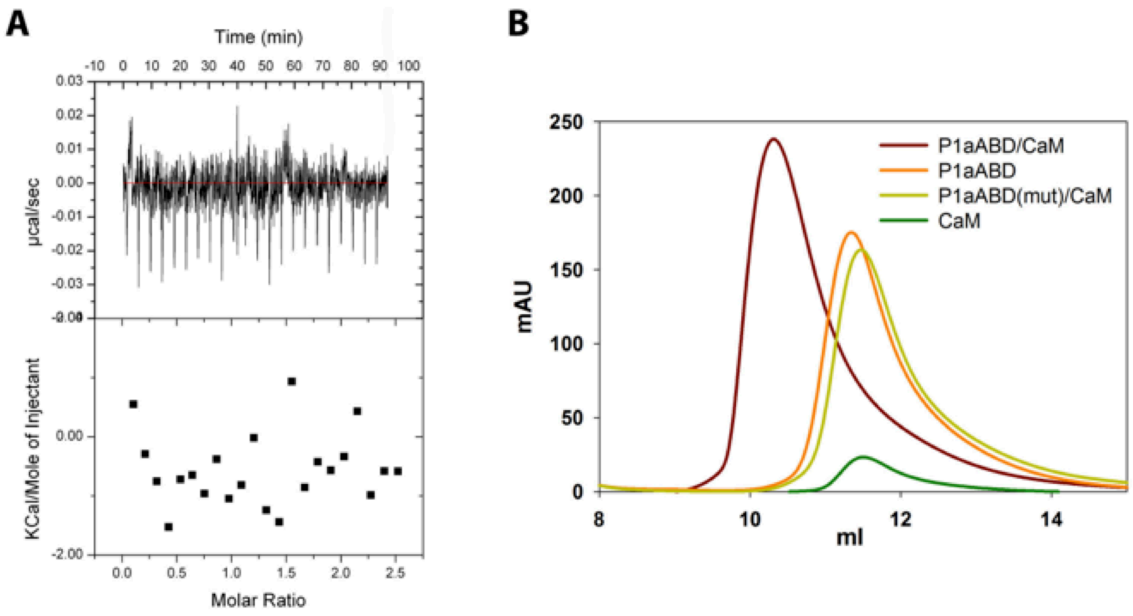

215

216 ***Supplementary Figure 3. (Supporting Results section "Crystal Structure of the Plectin 1a ABD***

217 ***in Complex with Calmodulin N-ter Lobe" and Figure 2)***

218 *In vitro* mutational analyses. **(A)** ITC experiment was carried out to measure the mutational

219 effect on the interaction. CaM is titrated to the P1aABD mutant (Leu25Asp and Val29Asp); no

220 interaction is observed. **(B)** Gel-filtration analyses. When P1aABD is mixed with CaM, it is eluted

221 earlier than CaM and P1aABD, suggesting the complex formation in solution. However P1aABD

222 mutant is not able to associate with CaM.

223

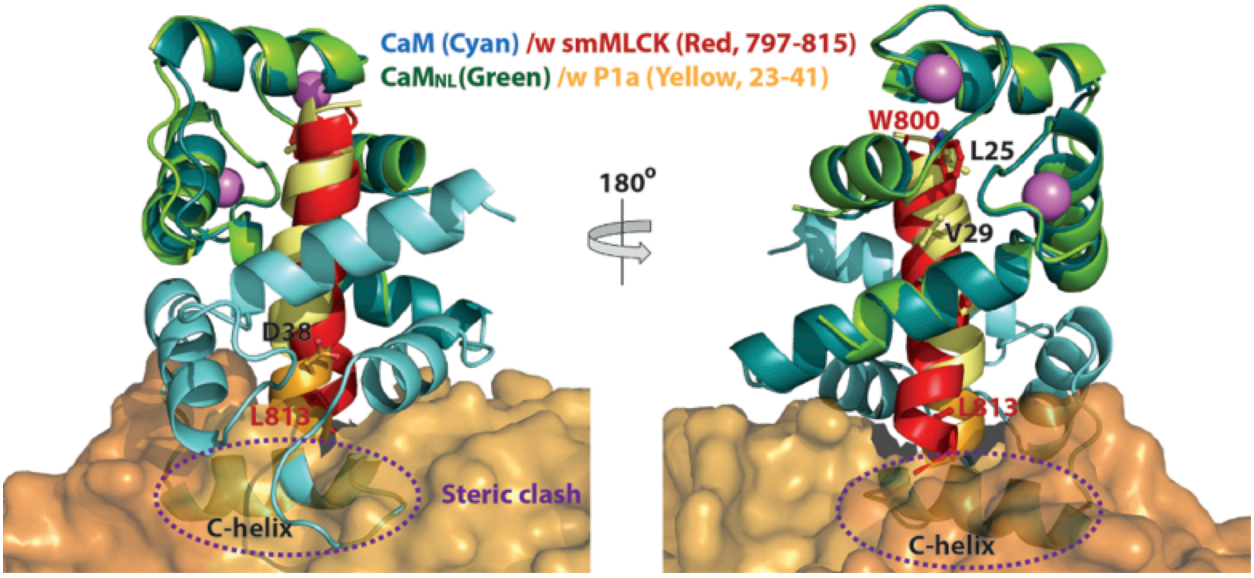

Supplementary Figure 4. (Supporting Results section "Calmodulin Binds to Plectin 1a in an Extended Conformation" and Figure 4)

The crystal structure of the P1aABD$_{\Delta 22}$/CaM$_{NL}$ complex superimposed on the crystal structure of the CaM/smMLCK complex (PDB:1CDL) (RMSD: 0.684Å over 57 Cα); N and C-lobes are respectively displayed in light and dark cyan and smMLCK peptide (797-815 residues) is shown in red. The superposition shows that C-helix of N-lobe makes a steric clash with plectin ABD (shown in an bronze (CH1) and orange (CH2) molecular surface).

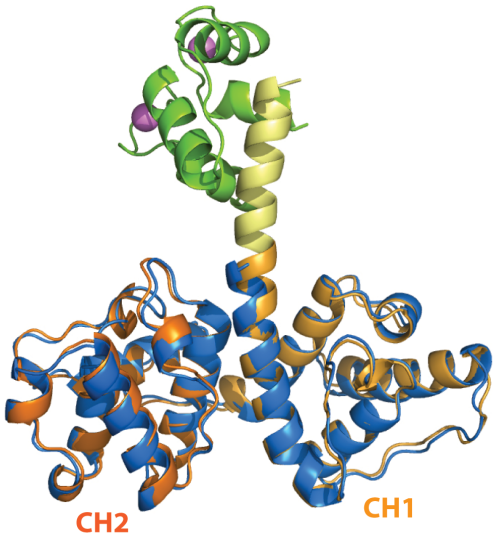

Supplementary Figure 5. (Supporting Results section "Plectin 1a N-terminal Tail Folds upon Binding to Calmodulin" and Figure 4)

The crystal structure of P1aABD$_{\Delta 22}$ is shown in blue and superimposed to the P1aABD$_{\Delta 22}$/CaM$_{NL}$ complex (RMSD: 0.69 Å over 209 equivalent Cα atoms), demonstrating that the Ca^{2+}/CaM binding does not affect the conformation of plectin ABD.

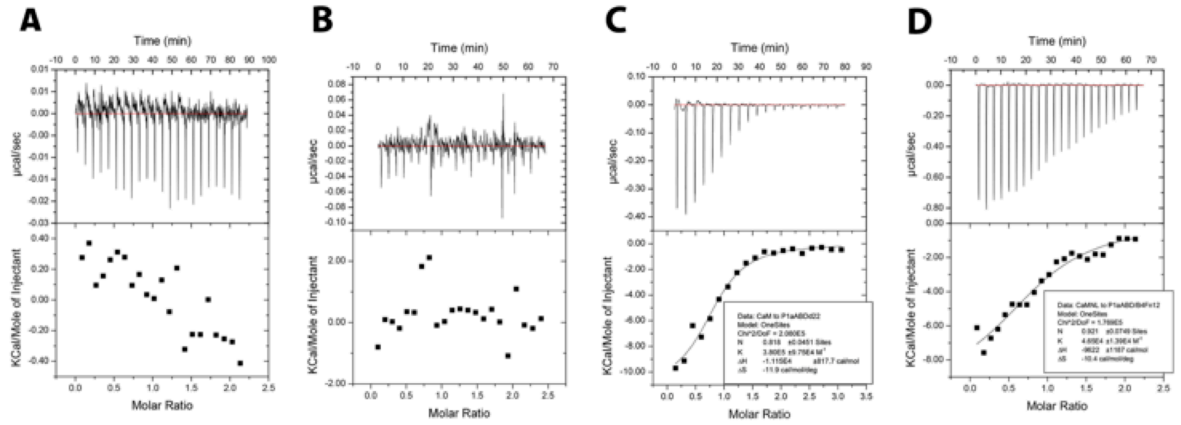

240

241 ***Supplementary Figure 6. (Supporting Results section "N-terminal Tail of Plectin 1a is not***

242 ***Involved in Interaction with Integrin β4" and Figure 7)***

243 ITC analyses **(A)** β4Fn12 (0.04 mM) was titrated with peptide comprising the first 60 N-terminal

244 residues of P1a (0.4 mM) at 30°C, displaying the no interaction. **(B)** β4Fn12 (0.04 mM) was

245 titrated with CaM (0.4 mM) at 30°C, displaying the no interaction. **(C)** P1aABD$_{\Delta 22}$ (0.02mM) was

246 titrated with CaM (0.3 mM); ITC experiment was carried out at 25 °C. The binding affinity of

247 P1aABD$_{\Delta 22}$ to CaM (K_d: 2.6 ± 1.0 µM) is similar to that of P1aABD. **(D)** P1aABD/β4Fn12 complex

248 (0.07 mM) was titrated with CaM$_{NL}$ (0.7 mM); ITC experiment was carried out at 30 °C. CaM$_{NL}$

249 bound to P1aABD in the presence of β4Fn12 with lower affinity (K_d: 21.5 ± 7.2 µM).

250

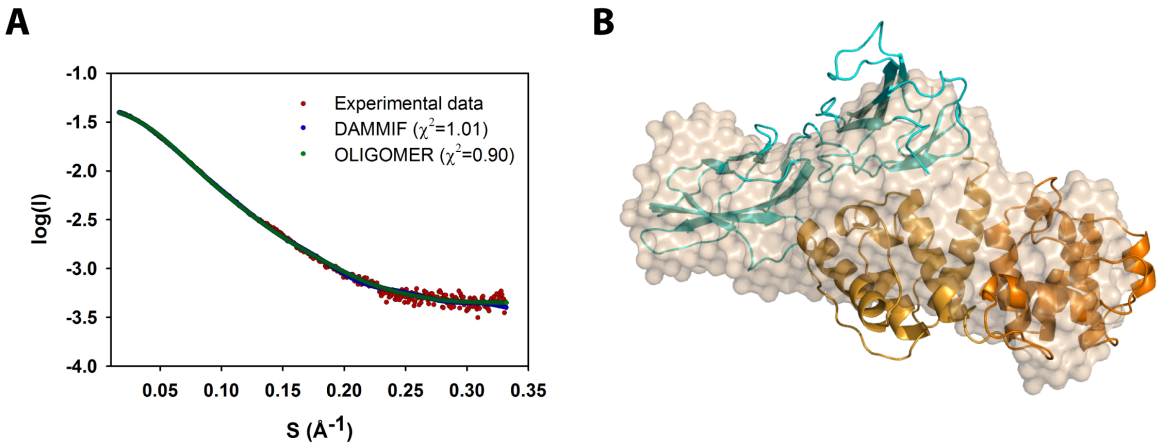

Supplementary Figure 7. (Supporting Results section "N-terminal Tail of Plectin 1a is not Involved in Interaction with Integrin β4" and Figure 6)

(A) SAXS curves. The experimental scattering curve of the P1ABD/β4Fn12 complex is shown in red. An *ab initio* model was fitted to experimental data and is shown in blue. The scattering profile of the crystal structure of the P1aABD$_{\Delta 22}$/β4Fn12 complex supplemented with missing residues was calculated using OLIGOMER and is displayed in green. **(B)** The crystal structure of the P1aABD$_{\Delta 22}$/β4Fn12 complex superimposed on the *ab initio* shell reconstructed from SAXS data .

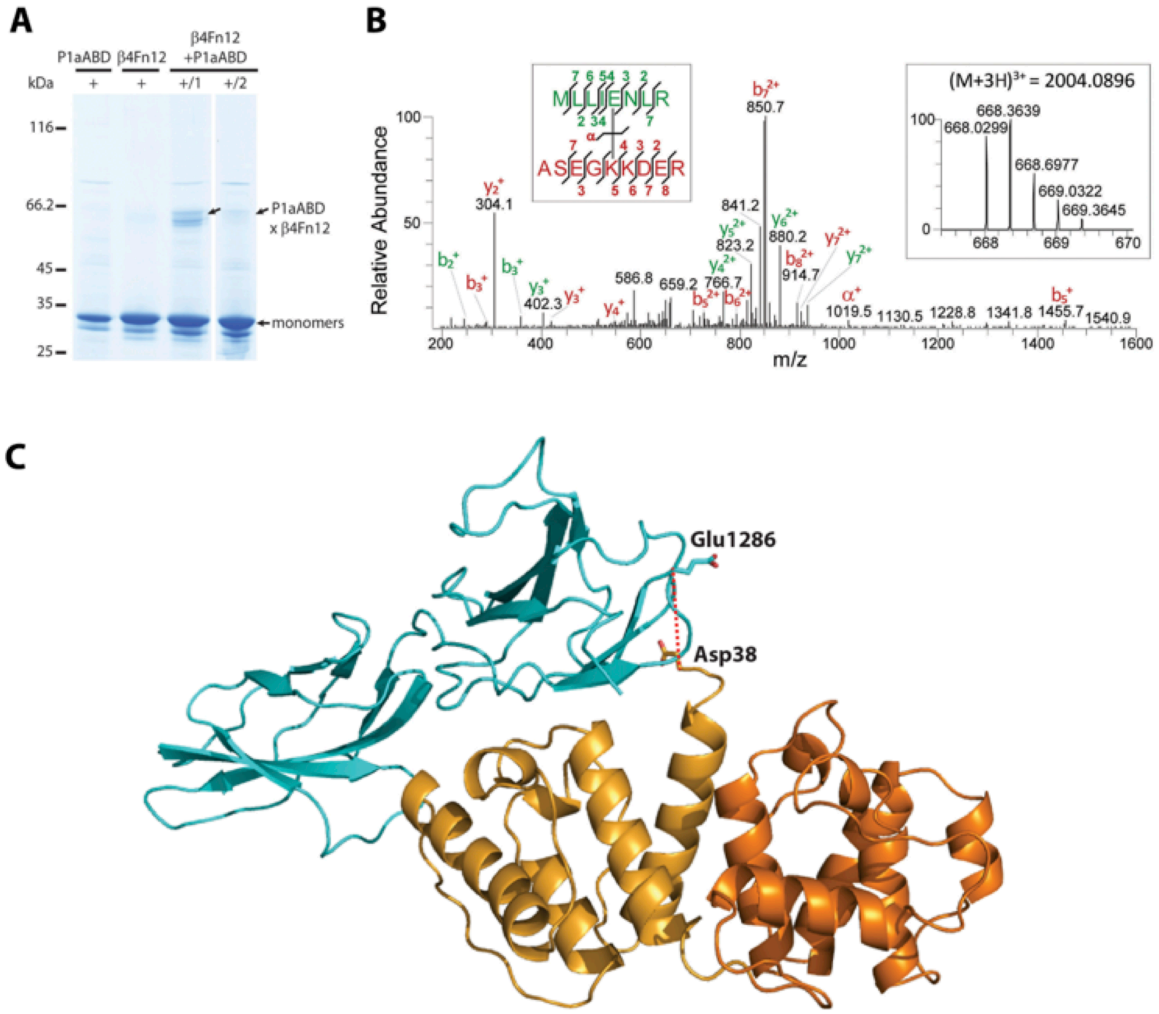

Supplementary Figure 8. (Supporting Results section "N-terminal Tail of Plectin 1a is not Involved in Interaction with Integrin β4" and Figure 6)

(A) SDS-PAGE analysis of β4Fn12/P1ABD complex cross-linked by zero-length chemical cross-linker EDC and sulfo-NHS. Proteins were incubated separately with cross-linker (+), in a one-step (+/1) or in a two-step (+/2) reaction activating β4Fn12. **(B)** MS/MS-Spectrum identifying a pair of cross-linked peptides after in-gel proteolysis of the P1ABD/β4Fn12 complex. **(C)** Crystal structure of the P1aABD/β4Fn12 shows that the cross-linking and MS results are consistent with the crystal structure. A distance between two Cα atoms (integrin β4 Glu1286 and plectin Asp38) is 12.97 Å.

A

N-lobe	9	IAEFKEAFSLFDKDGDGTITTKELGTVMRSLGQ	41
C-lobe	82	EEEIREAFRVFDKDGNGYISAAELRHVMTNLGE	114
	42	NPTEAELQDMINEVDADGNGTIDFPEFLTMMA	73
	115	KLTDEEVDEMIREADIDGDGQVNYEEFVQMMT	146

B

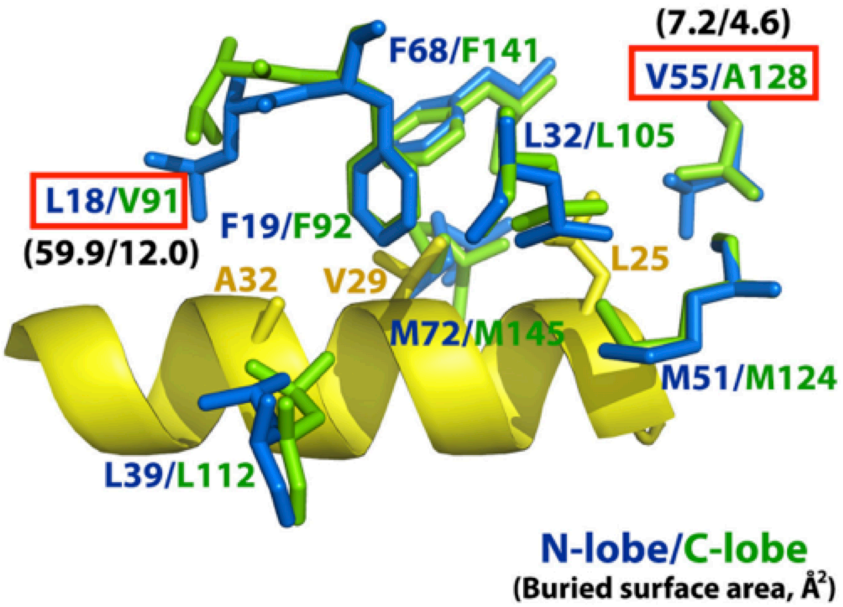

271

272 ***Supplementary Figure 9. (Supporting Results section "Molecular Determinants of Integrin β4***
273 ***Displacement from the Complex with Plectin 1a by Calmodulin")***

274 **(A)** The sequence alignment of each lobe of CaM. The interfacing residues were analyzed by
275 PDBePISA and shaded in yellow. Different residues between two lobes are shown in red **(B)**
276 Interfacing hydrophobic residues of two lobes determined by Ligplot are superimposed and
277 shown in sticks; N-lobe in blue and C-lobe in green, showing that Leu18 (59.9 $Å^2$) and Val55 (7.2
278 $Å^2$) in N-lobe offer a larger surface areas than Val91 (12.0 $Å^2$) and Ala128 (4.6 $Å^2$) in C-lobe.
279 Hydrophobic residues of P1a corresponding to a 1-5-8 motif (Leu25-Val29-Ala32) are displayed
280 in yellow.

References

Babu, Y.S., Bugg, C.E., and Cook, W.J. (1988). Structure of calmodulin refined at 2.2 A resolution. J Mol Biol *204*, 191-204.

Bernado, P., Mylonas, E., Petoukhov, M.V., Blackledge, M., and Svergun, D.I. (2007). Structural characterization of flexible proteins using small-angle X-ray scattering. J Am Chem Soc *129*, 5656-5664.

Blanchet, C.E., Zozulya, A.V., Kikhney, A.G., Franke, D., Konarev, P.V., Shang, W.F., Klaering, R., Robrahn, B., Hermes, C., Cipriani, F*., et al.* (2012). Instrumental setup for high-throughput small- and wide-angle solution scattering at the X33 beamline of EMBL Hamburg. J Appl Crystallogr *45*, 489-495.

Cox, J., Neuhauser, N., Michalski, A., Scheltema, R.A., Olsen, J.V., and Mann, M. (2011). Andromeda: a peptide search engine integrated into the MaxQuant environment. J Proteome Res *10*, 1794-1805.

Cristodero, M., Mani, J., Oeljeklaus, S., Aeberhard, L., Hashimi, H., Ramrath, D.J., Lukes, J., Warscheid, B., and Schneider, A. (2013). Mitochondrial translation factors of Trypanosoma brucei: Elongation factor-Tu has a unique subdomain that is essential for its function. Mol Microbiol.

David, G., and Perez, J. (2009). Combined sampler robot and high-performance liquid chromatography: a fully automated system for biological small-angle X-ray scattering experiments at the Synchrotron SOLEIL SWING beamline. J Appl Crystallogr *42*, 892-900.

Franke, D., and Svergun, D.I. (2009). DAMMIF, a program for rapid ab-initio shape determination in small-angle scattering. J Appl Crystallogr *42*, 342-346.

Geer, L.Y., Markey, S.P., Kowalak, J.A., Wagner, L., Xu, M., Maynard, D.M., Yang, X., Shi, W., and Bryant, S.H. (2004). Open mass spectrometry search algorithm. J Proteome Res *3*, 958-964.

Konarev, P.V., Volkov, V.V., Sokolova, A.V., Koch, M.H.J., and Svergun, D.I. (2003). PRIMUS: a Windows PC-based system for small-angle scattering data analysis. J Appl Crystallogr *36*, 1277-1282.

Kostan, J., Gregor, M., Walko, G., and Wiche, G. (2009). Plectin isoform-dependent regulation of keratin-integrin alpha6beta4 anchorage via Ca2+/calmodulin. The Journal of biological chemistry *284*, 18525-18536.

Krissinel, E., and Henrick, K. (2007). Inference of macromolecular assemblies from crystalline state. J Mol Biol *372*, 774-797.

Niessen, C.M., Hulsman, E.H., Oomen, L.C., Kuikman, I., and Sonnenberg, A. (1997). A minimal region on the integrin beta4 subunit that is critical to its localization in hemidesmosomes regulates the distribution of HD1/plectin in COS-7 cells. J Cell Sci *110 (Pt 15)*, 1705-1716.

Petoukhov, M.V., Franke, D., Shkumatov, A.V., Tria, G., Kikhney, A.G., Gajda, M., Gorba, C., Mertens, H.D.T., Konarev, P.V., and Svergun, D.I. (2012). New developments in the ATSAS program package for small-angle scattering data analysis. J Appl Crystallogr *45*, 342-350.

Rezniczek, G.A., de Pereda, J.M., Reipert, S., and Wiche, G. (1998). Linking integrin alpha6beta4-based cell adhesion to the intermediate filament cytoskeleton: direct interaction between the beta4 subunit and plectin at multiple molecular sites. J Cell Biol *141*, 209-225.

Schlosser, A., Vanselow, J.T., and Kramer, A. (2007). Comprehensive phosphorylation site analysis of individual phosphoproteins applying scoring schemes for MS/MS data. Anal Chem *79*, 7439-7449.

Stanek, D., and Neugebauer, K.M. (2004). Detection of snRNP assembly intermediates in Cajal bodies by fluorescence resonance energy transfer. J Cell Biol *166*, 1015-1025.

Svergun, D. (1992). Determination of the regularization parameter in indirect-transform methods using perceptual criteria. J Appl Crystallogr *25*, 495-503.

Volkov, V.V., and Svergun, D.I. (2003). Uniqueness of ab initio shape determination in small-angle scattering. J Appl Crystallogr *36*, 860-864.